

Impact of patient, surgical, and implant design factors on predicted tray–bone interface micromotions in cementless total knee arthroplasty

Huizhou Yang | Riza Bayoglu  | Chadd W. Clary  | Paul J. Rullkoetter 

Center for Orthopaedic Biomechanics,
University of Denver, Denver, Colorado, USA

Correspondence

Paul J. Rullkoetter, Center for Orthopaedic Biomechanics, University of Denver, Room 427, 2155 E. Wesley Ave., Denver, CO 80208, USA.
Email: paul.rullkoetter@du.edu

Funding information

DePuy Synthes

Abstract

Micromotion magnitudes exceeding 150 μm may prevent bone formation and limit fixation after cementless total knee arthroplasty (TKA). Many factors influence the tray–bone interface micromotion but the critical parameters and sensitivities are less clear. In this study, we assessed the impacts of surgical (tray alignment, tibial coverage, and resection surface preparation), patient (bone properties and tibiofemoral kinematics), and implant design (tray feature and surface friction) factors on tray–bone interface micromotions during a series of activities of daily living. Micromotion was estimated via three previously validated implant–bone finite element models and tested under gait, deep knee bending, and stair descent loads. Overall, the average micromotion across the tray–bone cementless contact interface ranged from 9.3 to 111.4 μm , and peak micromotion was consistently found along the anterior tray edge. Maximizing tibial coverage above a properly sized tibial tray (an average of 12.3% additional area) had minimal impact on micromotion. A 1 mm anterior tray alignment change reduced the average micromotion by an average of 16.1%. Two-degree tibial angular resection errors reduced the area for bone ingrowth up to 48.1%. Differences on average micromotion from $\pm 25\%$ changes in bone moduli were up to 75.5%. A more posterior tibiofemoral contact due to additional 100 N posterior force resulted in an average of 79.3% increase on average micromotion. Overall, careful surgical technique, patient selection, and controlling kinematics through articular design all contribute meaningfully to minimizing micromotion in cementless TKA, with centralizing the load transfer to minimize the resulting moment at the anterior tray perimeter a consistent theme.

KEY WORDS

cementless, finite element analysis, fixation, micromotion, total knee arthroplasty

1 | INTRODUCTION

As the number of younger and more active patients treated with total knee arthroplasty (TKA) continues to increase,^{1,2} implants are required to carry potentially greater dynamic activity cycles while maintaining long-term durability.³ Compared with cemented implants, current innovations in cementless tibial trays may offer a more long-lasting biological fixation.⁴ The initial fixation of cementless tibial trays after TKA is crucial to bony ingrowth into the porous surface of the implants,⁵ as micromotion magnitudes exceeding 150 µm may prevent bone formation and lead to implant loosening.^{6,7} Many factors, such as surgical alignment, prosthesis design choices, and patient differences may affect the tray–bone micromotion. Therefore, understanding the critical parameters impacting micromotion is required for optimal design, patient selection, and clinical performance.

In vitro experiments have been performed to investigate the impact of different TKA designs on tray–bone micromotion.^{8,9} These studies measured the relative displacements between markers placed on the exposed surfaces of the tray and bone. Typically, the full tray–bone interface is not accessible and therefore surface micromotion has not been fully quantified experimentally.^{10,11} Our prior study also indicated that these marker relative displacements did not numerically represent the actual micromotions at the contact surface.¹² Therefore, finite element models have been commonly used in combination to estimate the interface micromotion and to investigate factors that are generally infeasible to study via experimental methods. Previous in silico studies have primarily estimated the tray–bone micromotion under different loading conditions,^{13,14} although a few also investigated the micromotion sensitivity of key factors such as implant alignment, design features, or individual differences. Sopher et al. investigated the impact of the implant design and positioning on the implant–bone micromotion in total ankle replacement.¹⁵ Barker et al. virtually perturbed the circumferential flange of the tibial tray and predicted the influence on tray–bone shear micromotions.¹⁶ Hashemi and Shirazi-Adl compared the predicted micromotions between different fixation configurations of the tibial tray.¹⁷ The loading conditions applied in these TKA studies were typically simple vertical loads which do not account for the more complex physiological loading at the knee joint during daily activities. Glenday et al. studied the effect of varus alignment on the micromotion with consideration of the loading variations.¹⁸ However, the loading was applied to the center of tibial tray without consideration of physiological femoral-insert contact.

Our prior experimental–computational study has presented validation of predicted cementless tray–bone relative micromotions over a range of simulated activities of daily living for three implanted tibial bones.¹² In addition, we evaluated the impact of alignment and tray–bone friction on the interface micromotion. Several recent studies have reported that implant pegs have a considerable impact on tibial fixation.^{15–17} Additionally, maximizing tibial coverage is thought to improve fixation due to the more

uniform distribution of the forces.^{19–21} Plaskos et al. has reported that resection errors relative to the TKA cutting guide were in the range of 1.5~4.0° during bone preparation, which was foreseen to affect the tibial fixation.²² Differences in tibial elastic properties between samples with the same bone volume fraction have been reported to range up to 53% due to the different trabecular architectures.²³ Variations in tibiofemoral kinematics have also been reported due to the differences in surgical and patient characteristics.^{24,25} To our knowledge, no previous publications have systematically studied the sensitivity of the tray–bone micromotion to these factors under physiological conditions.

Hence, this study aimed to investigate the influence of surgical (tray alignment, tibial coverage, and resection surface preparation), patient (bone properties and tibiofemoral kinematics), and implant design (tray features and surface friction) factors on the tray–bone interface micromotions during a series of activities of daily living. Factors were studied using three previously validated tibia-implant models during simulated gait (GT), deep knee bending (DKB), and stair descent (SD). The tray–bone interface micromotion for each model was predicted and compared with the original configuration, and critical parameters were identified.

2 | METHODS

2.1 | Experimental setup and computational validation

The computational models used in this study were adopted from our previously published work.¹² Description of the experimental setups and model validations are briefly summarized here. Three cadaveric tibiae were implanted with cementless tibial prostheses (best-fit size, rotating-platform, cruciate-retaining, ATTUNE®, Depuy Synthes) by an experienced surgeon. Specimens were then cemented into custom fixtures and mounted in the 6-DoF AMTI VIVO™ knee simulator (AMTO) to simulate GT, DKB, and SD activities. Experimental boundary conditions were derived from telemetric implant data and ASTM standard.²⁶ Consistent boundary conditions (loading and kinematics) were applied to each simulated specimen. Flexion/extension (FE) and internal/external rotation (IE) degrees of freedom (DoFs) were kinematically driven while medial/lateral (ML), anterior/posterior (AP), superior/inferior (SI), and varus/valgus (VV) DoFs were load controlled. After bedding-in under cyclic compression for 200 cycles, 40 cycles of each activity were performed at a rate of 0.33 Hz. Relative displacements between marker couples (placed at the anterior aspects of the tray and bone) and tibial surface displacements were recorded with a digital image camera (DIC) system (Figure 1).

Corresponding computational models of the three specimens were developed in Abaqus/Standard (SIMULIA) from computed tomography (CT) scans with bone mineral density phantoms. Elastic moduli of the tibial elements were assigned based on Hounsfield units using established relationships.^{27,28} Component alignment

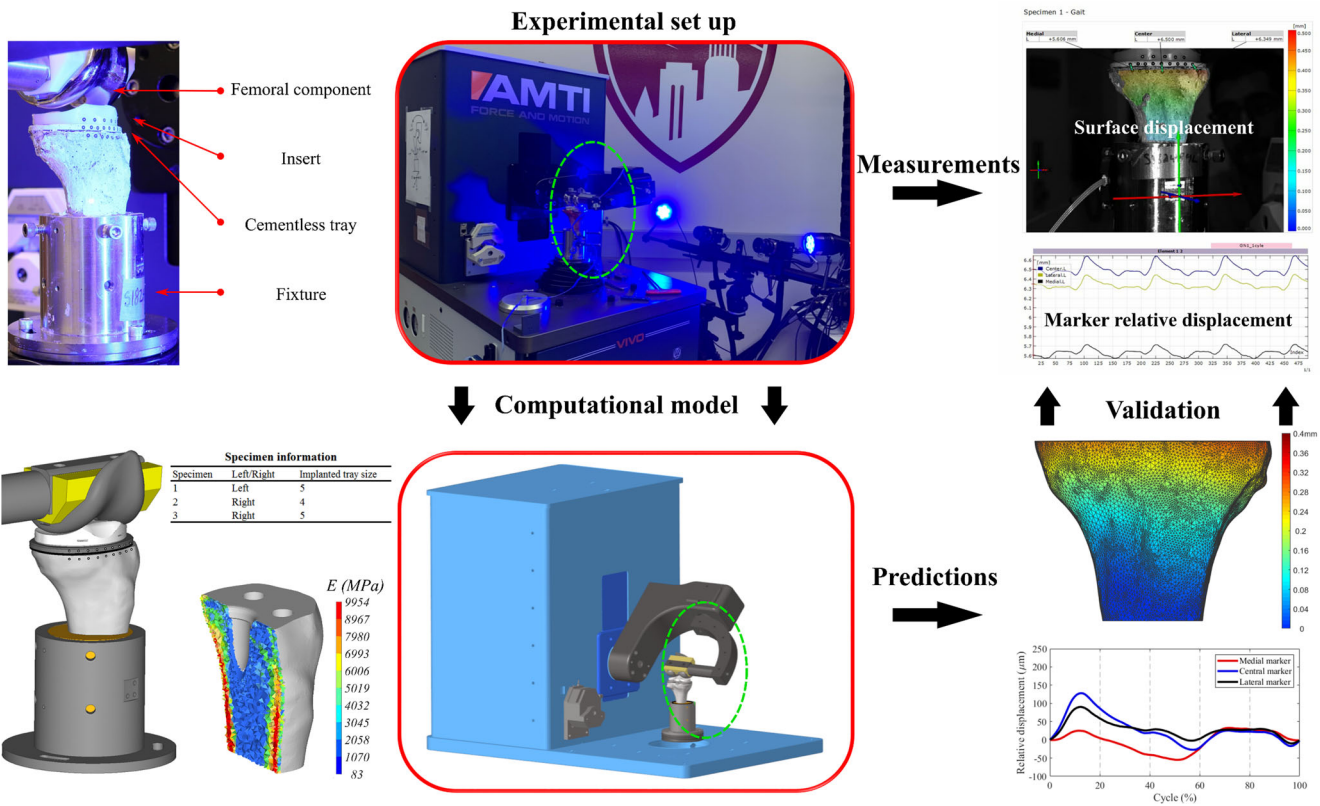


FIGURE 1 Computational–experimental validation framework. [Color figure can be viewed at wileyonlinelibrary.com]

and marker locations were reconstructed from the experiments. The deformable implant–bone construct was virtually mounted into the VIVO simulator model²⁹ and loaded via a rigid femoral component with the boundary conditions adopted from the VIVO experiment. The tray–bone interfaces were assumed to be line-to-line (no interference fit) and modeled with friction coefficients of 0.4 and 1.0 for solid–bone and porous–bone contact, respectively. The contact at the metal–poly (femoral–insert and insert–tray) interfaces were modeled with friction coefficients of 0.04. The marker and bone surface displacements were predicted and compared with experimental measurements (Figure 1). Prior convergence studies were completed during model development (including mesh size, the minimum number of simulated cycles required to reach a steady state, and the number of the material cards to characterize tibia properties). The average root-mean-square differences and correlations between measured marker relative displacements and predictions were 13.1 and 0.86 μm , respectively.

2.2 | Micromotion sensitivity research framework

The three validated cadaveric tibia–implant models were utilized for this follow-up study investigating the sensitivities of tray–bone interface micromotions to several common TKA factors. All boundary conditions (tray–bone alignment, activity loading,

femoral–insert initial positions, etc.) were consistent with the prior study unless being perturbed when studying specific factors. To differentiate with the perturbed models investigating micromotion sensitivities, the three original, validated models were indicated as “baseline models” subsequently. For each factor studied, the change of the factor was incorporated into each baseline model and the newly generated model was retested during GT, DKB, and SD.

The parameters of each factor and corresponding model configurations are as below:

2.3 | SURGICAL PARAMETERS

2.3.1 | Tray–bone alignment

For each baseline model, 19 models were developed by perturbing the initial tray–bone alignment (considering one perturbation at a time) ± 0.5 and ± 1.0 mm in all translational DoFs (AP, ML, and SI), $\pm 0.5^\circ$ and $\pm 1.0^\circ$ in IE DoF, $\pm 3.0^\circ$ in VV DoF, and 5.0° in FE DoF (resulting in a 5° tibial posterior slope) (Figure 2A). The perturbation choices considered that AP, ML, and IE tray–bone alignments are likely small given a properly sized and implanted tray, whereas VV and tibial slope alignments are more variable. After evaluating the impact of each parameter on the interface micromotion, an upper bound model configuration was developed by considering all

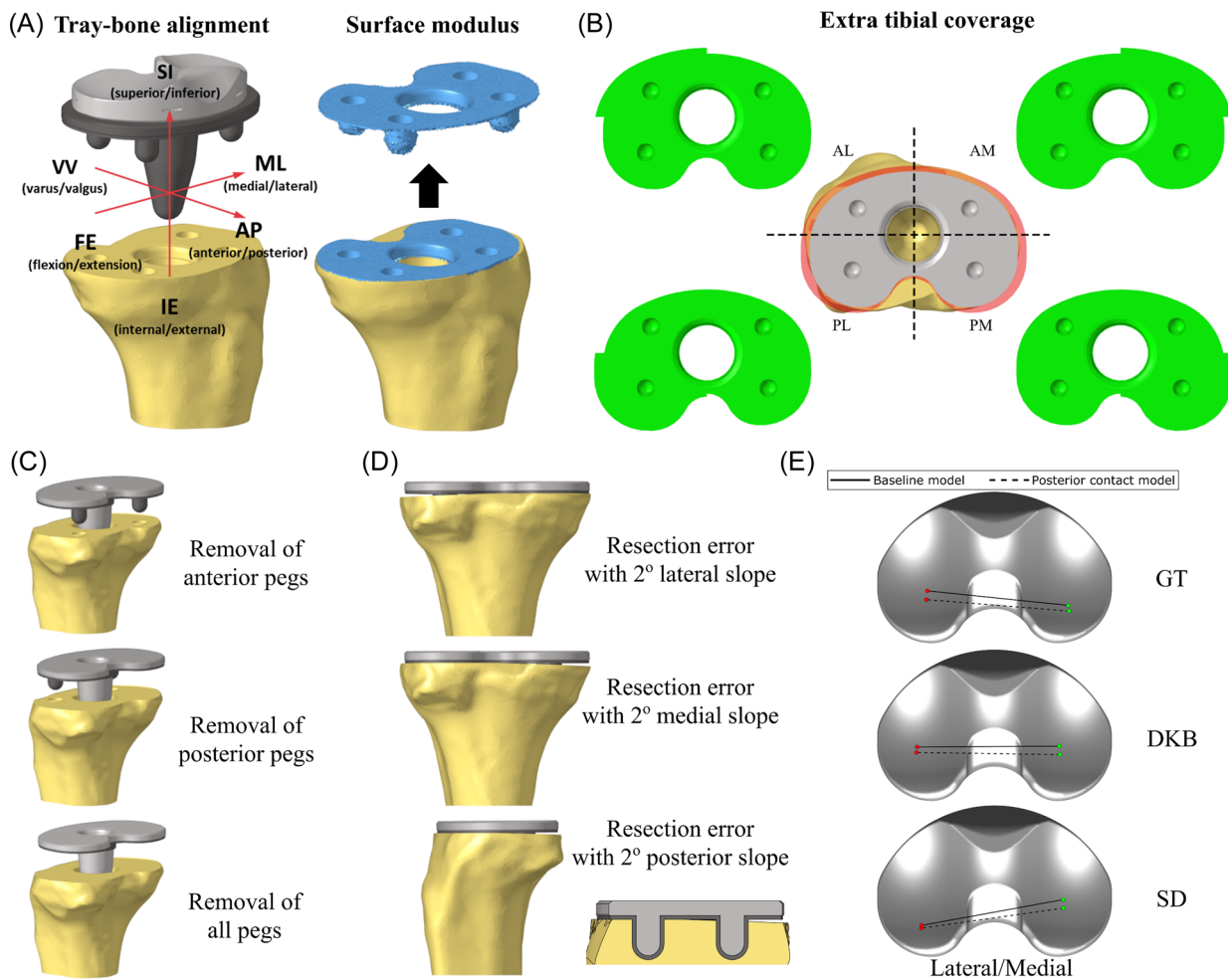


FIGURE 2 Illustration of the perturbation models for micromotion sensitivity tests (using a left tibia sample). (A) Tray–bone alignment perturbations and the isolated elements for calculating tibial surface modulus. (B) Region divisions of the tibial coverage (AL, anterolateral; AM, anteromedial; PL, posterolateral; PM, posteromedial). Five virtual tray models with extra tibial coverages (gray, original tray; green, trays with extra coverage in each quadrant; red, tray with extra coverage in all regions). (C) Tray and tibial models for studying the impact of tray pegs. (D) Tibial models with 2°-slope resection errors. (E) Differences in tibiofemoral AP translations between baseline models and posterior-contact models (+100 N posterior load) at peaking micromotion frames. [Color figure can be viewed at wileyonlinelibrary.com]

the parameters (a combination of six DoFs perturbations) which resulted in higher micromotions. Similarly, a lower bound model configuration was developed.

For each perturbation model, the changes in tibial contact surface modulus due to the realignments were investigated with consideration of the potential impact on micromotion. The tibial surface elements near the tray (distance from the tibial element center to the tray surface < 0.75 mm) were isolated and the average elastic modulus of those elements was calculated (Figure 2A). As certain component alignment alters the tibiofemoral loading conditions,³⁰ we evaluated the loading/kinematics variations due to the implant positioning by using a previously validated lower limb model.³¹ The changes in loading conditions are shown in Figure 3 for VV and tibial slope alignments (the changes due to the other perturbations were negligible) and were incorporated into the micromotion simulations.

2.3.2 | Tibial coverage

To best understand the isolated impact of tibial coverage on micromotion, we virtually increased the porous coating area to achieve the maximum coverage. For each baseline model, the porous coating of the cementless tray was divided into four regions, anterolateral, anteromedial, posterolateral, and posteromedial (Figure 2B). The covered tibial area in each region was recorded. Four tray models were virtually created to achieve more coverage in each region (Figure 2B). Another model was created by enlarging the entire geometry (a combination of the previous four models), which had the same coverage area as using a two-size-larger tray. However, it should be noted that this was not completely equivalent to using a larger tray because the peg positions were unchanged. Thus, the impact of the tibial coverage was isolated. It should be also noted that overhang of the tibia is not clinically acceptable. For modeling convenience, we

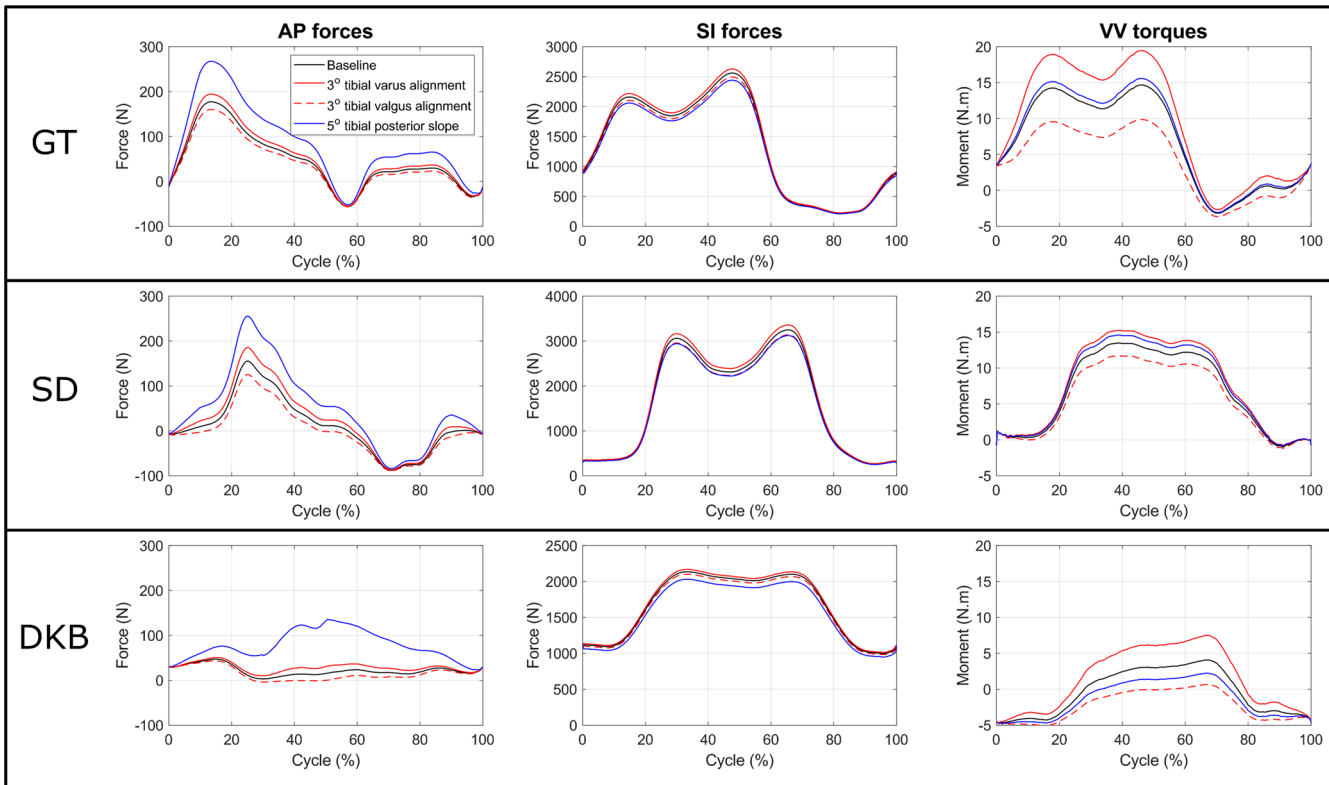


FIGURE 3 Variations in the loading conditions due to 3° varus/valgus alignment and 5° tibial posterior slope. DKB, deep knee bending; GT, gait; SD, stair descent. [Color figure can be viewed at wileyonlinelibrary.com]

ignored the overhangs when creating these tray models since the overhang has no impact on the predicted micromotion.

2.3.3 | Tibial angular resection error

Each baseline tibial model was additionally resected with a 2° medial, lateral, and posterior slope, respectively, to simulate an angular resection error during the tibial preparation. The slopes started from the center of the tray stem and the bottom of the pegs remained fully contacted with the tibia (a small portion of the peg surfaces was exposed, see Figure 2D). The scenario with an anterior slope resection error was not simulated since the anterior tibia is much more visible during the tibial preparation, so that the anterior tibia is more likely to be flat. The scenarios with resection errors resulting in more bone remaining (caused by the cutting blade deflecting upward) were also not considered since the tray would still have sufficient support at the edges, which should not be worse than the simulated cases.

2.4 | DESIGN PARAMETERS

2.4.1 | Porous tray–bone coefficient of friction

Based on test data from the manufacturer, the coefficient of friction was defined as 1.00 at the porous tray–bone interface for the

baseline models. To study the impact of this factor, this coefficient of friction was perturbed from 0.6 to 1.4 (with a 0.2 increment) to cover a wide range of potential variability.

2.4.2 | Tray pegs

For each baseline model, three alternative models of the tray were created by removing the anterior pegs, posterior pegs, and all pegs, respectively. The corresponding tibial models were also recreated with the same changes in tray geometries (Figure 2C).

2.5 | PATIENT FACTORS

2.5.1 | Tibiofemoral AP/IE load/kinematics

Deviations in tibiofemoral AP translation of approximately ± 2.6 mm and up to 15.78° tibial internal rotation during flexion were reported among patients for cruciate-retaining and rotating platform TKAs.^{24,25} For each activity, the AP forces through the activity were smoothly amplified by a ratio so that the peak force pushing the femur posterior was 50, 100, and 150 N larger, respectively, whereas the profile of the loading was unchanged (the sign of the force was unchanged for any frame). All the baseline models were retested under these new loading conditions. The changes in tibiofemoral

positioning due to changes in tibiofemoral internal-external rotations were also considered. The input IE kinematics were smoothly amplified so that the internal rotation of the tibia at the frame having peak micromotion was 5 and 10° larger (resulting in a more posterior contact position on the lateral condyle). These applied perturbation values were chosen so that the resulting AP translation and the tibial internal rotation were within the reported ranges but approaching the boundaries.

2.5.2 | Bone material property

As the density-modulus relationship used in the validated baseline models was approximately average of the reported range of tibial properties,^{27,28,32–35} we perturbed the elastic modulus of the baseline tibial models by ±25% to cover reported variations in tibial elastic properties.²³

Overall, a total of 132 models (3 baseline and 129 perturbation models) were created and 396 simulations (139 models tested under 3 loading conditions) were run to complete this study.

2.6 | Data analysis

In this study, we defined the tray–bone interface micromotion as the relative motions between the tray and the tibia contact surface. In computational models, the change in the distance (considering both shear and normal components) between the nodes at the tray bottom surface and the nearest node on the tibia implantation surface were used to represent the tray–bone interface micromotion. For each model, the micromotion at the tray–bone interface was predicted through the entire activity cycle. The full-field micromotion contour map for the frame having the peak micromotion is presented. The average and maximum value of the interface micromotions through the entire activity cycle were compared with the corresponding baseline model, and the impact of each factor on micromotion was determined.

In addition, we divided the tibial coverage area into three regions: micromotion less than 50 µm (ideal for bone ingrowth), micromotion ranging from 50 to 150 µm, and micromotion exceeding 150 µm (inhibiting bone formation).^{6,7} For each model, the coverage ratio of each region was calculated to provide a more comprehensive view of the fixation stability.

3 | RESULTS

For visualization of the resulting micromotion variations, the full-field interface micromotion contour maps are presented for the first specimen during GT activity (GT always had the highest micromotions), which covered the typical configurations for all factors (Figure 4). The patterns of the micromotion distributions during DKB and SD activities were similar but different in magnitude.

Overall, peak micromotion was consistently found along the anterior edge of the tray for all activities and ranged from 33.9 (Specimen 1 during DKB activity with the removal of all pegs) to 572.3 µm (Specimen 2 during GT activity with an additional 150 N posterior force). The peak magnitude (572.3 µm) does not provide a complete picture of the micromotion, as over 70% of the interface had micromotion less than 150 µm (for a graphic reference, Figure 3—tibiofemoral AP translation). Coverage ratios of the three fixation levels are presented in for the second specimen during GT activity (which had the highest percentage of micromotion exceeding 150 µm among all specimens and activities) (Figure 5).

3.1 | Surgical parameters

3.1.1 | Tray–bone alignment

For all specimens and activities, perturbations of the tray alignments along the AP translational and VV rotational DoFs resulted in an average change of 20.6% (16.1%) and 13.4% (10.9%) in peak and average micromotions per 1.0 mm or 3.0° variations. Values in round brackets represent the changes in *average* micromotions, and this is the same for the following results. The average changes caused by perturbations along the other directions were much smaller (ML: 4.8% [3.0%]; SI: 5.8% [4.4%]; FE: 5.4% [4.1%]; IE: 3.6% [1.8%]) (Figure 6A). The tibial surface modulus was almost unchanged except when perturbing the tray alignment along the SI direction (Figure 6B). The average change in contact modulus for each quadrant was 5.1 MPa (2.1%) and the maximum change was less than 10.0% except for SI perturbations. Implanting the tray more superiorly resulted in a stiffer engagement, while implanting the tray more inferiorly resulted in a softer engagement. The phenomenon was most pronounced for the first specimen, which led to a larger impact of the tray alignment along the SI direction on the micromotion compared with the other two specimens. Specifically, within the bounds of the perturbations studied, implanting the tray anteriorly, superiorly, or increasing the tibial valgus alignment always resulted in lower interface micromotions for all specimens.

For the six-DoF-perturbation bound models, the peak micromotions predicted from the upper bound models were on average of 130.9% (123.4%), 85.9% (42.4%), and 141.4% (127.5%) larger than those predictions from the lower bound models during GT, DKB, and SD activities, respectively (Figure 6C). The corresponding changes in the region experiencing micromotion more than 150 µm were up to 19.7% (Figure 5). The micromotions during the DKB activity were significantly smaller in magnitude than those in GT and SD activities.

3.1.2 | Tibial coverage

For all specimens, considerable increments in tibial coverage were achieved by using the enlarged tray models (Figure 7, top). When

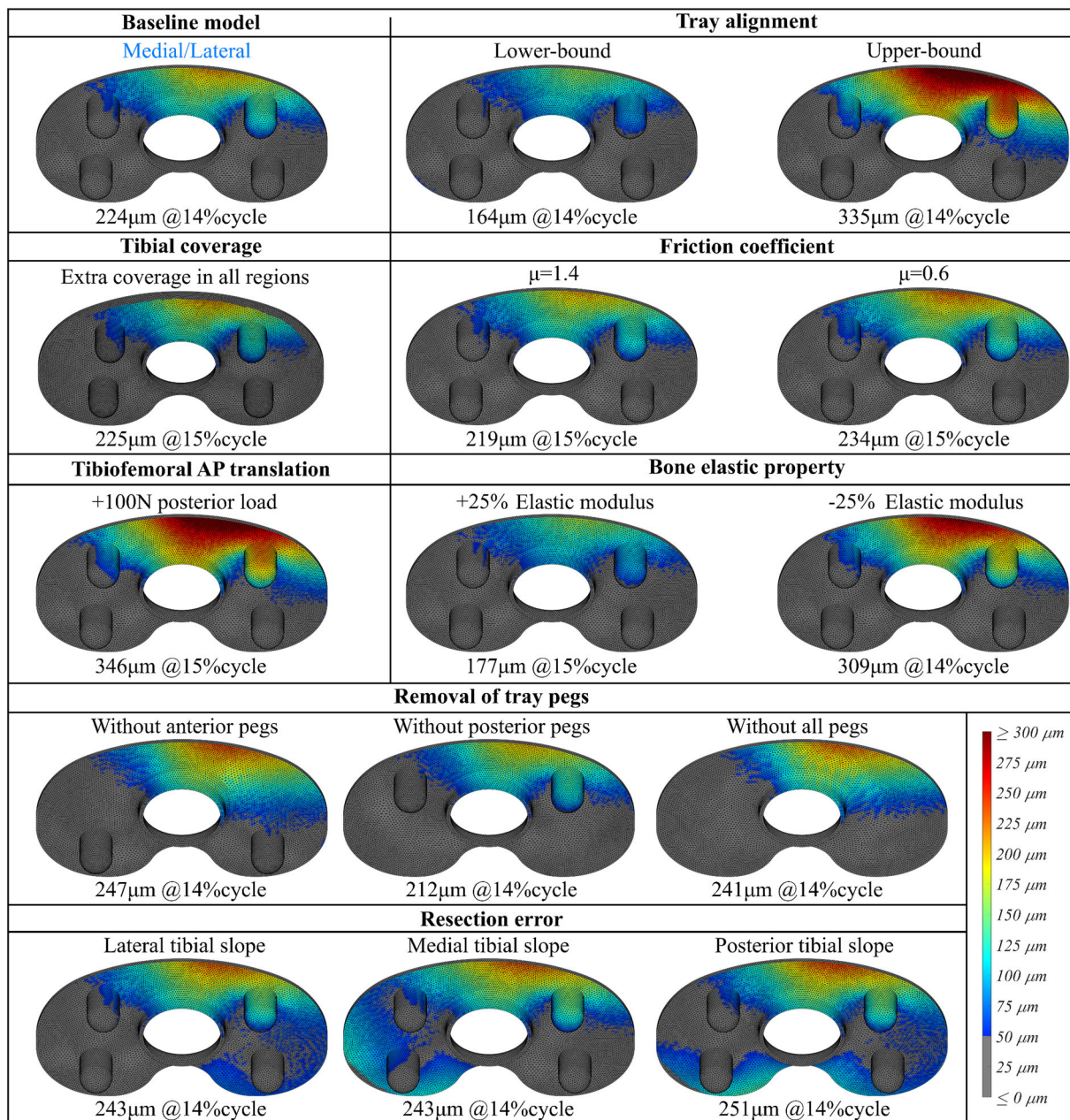


FIGURE 4 The predicted full-filled interface micromotion contour maps at the frames having peak micromotion magnitudes for the baseline model and the typical perturbation models of each factor. (The presented plots were from the first specimen during gait activity.) AP, anterior/posterior. [Color figure can be viewed at wileyonlinelibrary.com]

using the tray model with extra coverage in all regions (an average of 12.3% additional area), the tibia was fully covered around the perimeter except the zone for the posterior cruciate ligament (Figure 2B). The average changes in the peak micromotion with the usage of these all-covered tray models were 0.7% (0.5%), 1.3% (0.7%), and 1.9% (0.9%) for Specimens 1, 2, and 3, respectively (Figure 7, bottom). The maximum change in micromotion was less than 4% (2%). It should be noted that the micromotion at the extra surface of the tray beyond bony contact were excluded from the results (Figure 4—tibial coverage) for the comparison.

3.1.3 | Tibial angular resection error

The impact of angular resection errors was substantial for the DKB activity (Figure 8A) but remained smaller than GT or SD activities. This was a result of relative motions of the unsupported regions greatly exceeded the small baseline micromotions at the anterior aspect (Figure 4—resection error). For all activities, the peak micromotions at the anterior aspect were increased by an average of 13.8% due to the instability introduced by the resection errors. However, the average micromotion increased by an average of

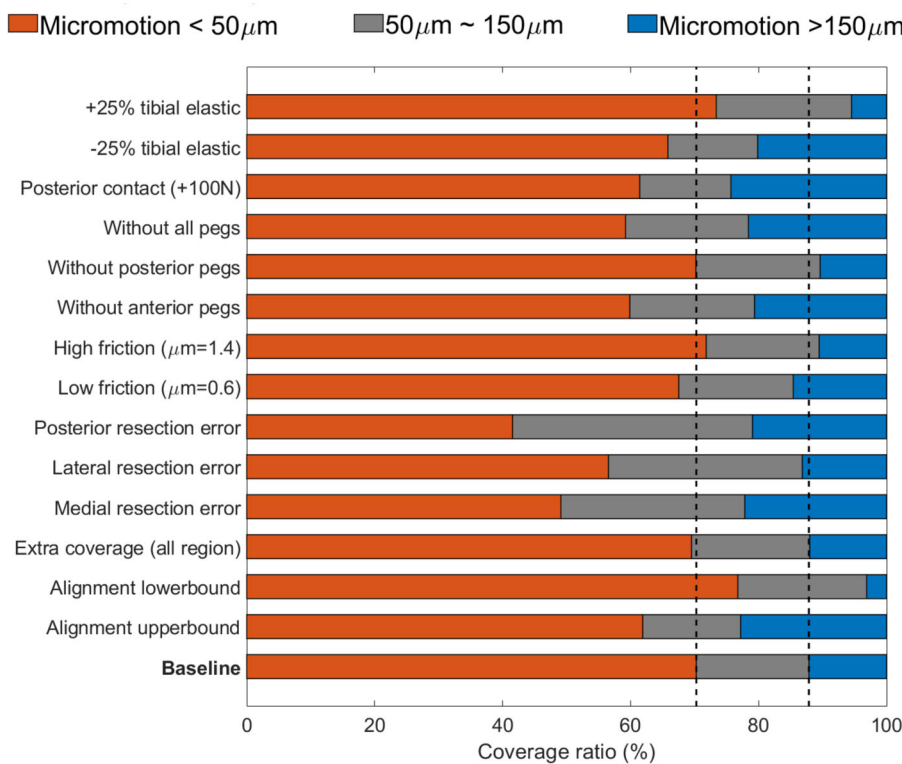


FIGURE 5 The coverage ratios of the three fixation levels at the tray–bone contact interface. (The presented plot was from the second specimen during gait activity.) [Color figure can be viewed at wileyonlinelibrary.com]

74.8% due to the significantly reduced area experiencing micromotion less than 50 μm . The impact was highest for a posterior angular resection error followed by medial, and lateral resection errors, however, at the same level. In addition, regions experiencing micromotion less than 50 μm reduced by an average of 33.5%, 16.3%, and 42.4% during GT, DKB, and SD, respectively, when a posterior angular resection error was created (Figure 5). These reductions in the ideal area for bone ingrowth (<50 μm) were more severe than those with a medial or lateral angular resection error (Table 1). For the micromotion at those unsupported regions, subsidence micromotion (results in gap-closing) accounted for 78% of the total micromotion.

3.2 | DESIGN PARAMETERS

3.2.1 | Tray–bone coefficient of friction

Overall the peak micromotions (occurred during GT among the three activities) reduced by an average of only 9.7% (15.1%) when increasing the coefficient of friction from 0.6 to 1.4 (the full range evaluated here) (Figure 8B).

3.2.2 | Tray pegs

The impact of tray pegs was small for the rotating-platform implant (Figure 8C). The anterior pegs play some role in restricting the tray

tilting motion at the anterior side (Figure 4—removal of tray pegs). The peak micromotions increased by an average of 11.1% with the removal of anterior pegs when the micromotion exceeded 150 μm (Specimens 1 and 2 during GT and SD). However, the removal of all pegs did not make these situations substantially worse. The peak micromotions only increased by an average of 13.3% with the removal of all pegs. For the implant studied, the cone provided the primary stability resisting micromotion. It should be noted that with the removal of peg geometries, the total cementless contact area reduced by 25%, which led to a higher increase in the average micromotion (22.2%) as the geometries removed had small micromotions.

3.3 | PATIENT FACTORS

3.3.1 | Tibiofemoral AP/IE load/kinematics

The changes in tibiofemoral contact positioning (at the frame having peak micromotion) due to the different AP forces and IE rotations are shown in Figure 9A for Specimen 1 (the patterns for Specimens 2 and 3 were similar). The medial and lateral contact locations moved posteriorly with increased posterior forces. A posterior tibiofemoral contact position due to a 100 N larger posterior force resulted in 54.8% (60.1%), 65.2% (71.2%), and 81.8% (82.7%) increases in the peak micromotions for Specimens 1, 2, and 3, respectively (Figure 9B). The medial-lateral contact rotated by a similar angle when the IE rotations were perturbed (Figure 9A). During DKB

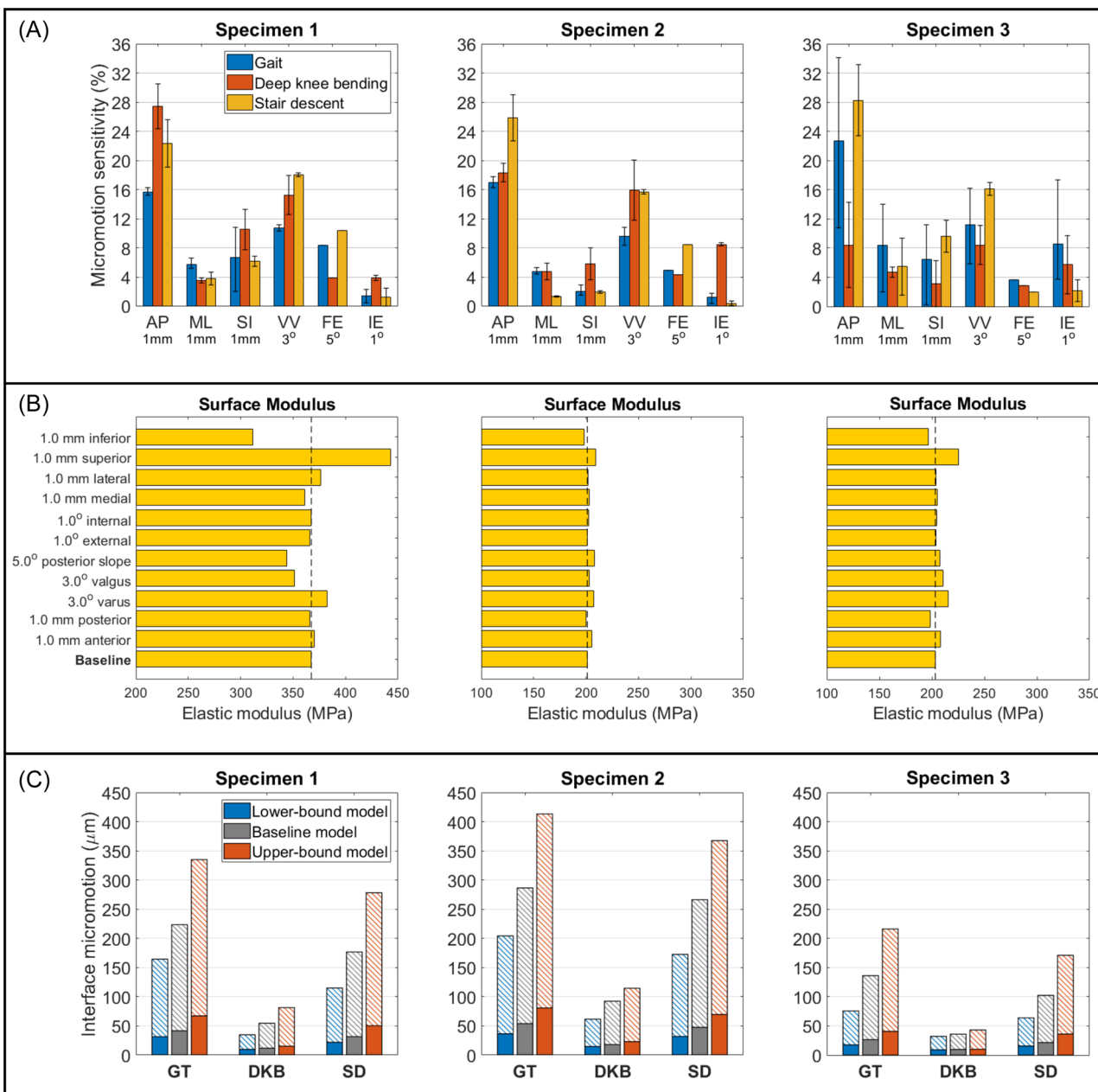


FIGURE 6 (A) The impact of tray alignment parameters on the interface micromotion with per 0.5 mm or degree perturbation. (B) Variations of the tibial surface modulus at the contact interface due to the changes in the tray–bone alignment. (C) Comparisons of the interface micromotions between the baseline models and the lower/upper bound models (combination of perturbing tray–bone alignment in six degrees of freedom [DoFs]). The hatched bars represent the peak micromotions and the solid bars represent the average micromotions. [Color figure can be viewed at wileyonlinelibrary.com]

activity, the lateral contact also moved posteriorly with increased tibial internal rotation. Peak micromotions were increased by an average of 198.5 μm during DKB activity but increases were much smaller during GT and SD activities (changed by an average of 24.7 μm) when the tibial internal rotation was increased by 10° (Figure 9C). For all models (with increased posterior force or increased tibial internal rotation), the micromotions were linearly related to the resulting moments as a result of the posterior positions evaluated ($R = 0.99$).

3.3.2 | Bone material property

The peak interface micromotions reduced by an average of 19.9% (17.1%) when the tibial material properties were increased by 25%, and micromotions increased by an average of 38.4% (34.3%) when the tibial material properties were decreased by 25% (Figure 9D).

For each factor, micromotions in normal and shear directions increased/decreased simultaneously, following the same trend as the total micromotions presented, where the normal micromotions were

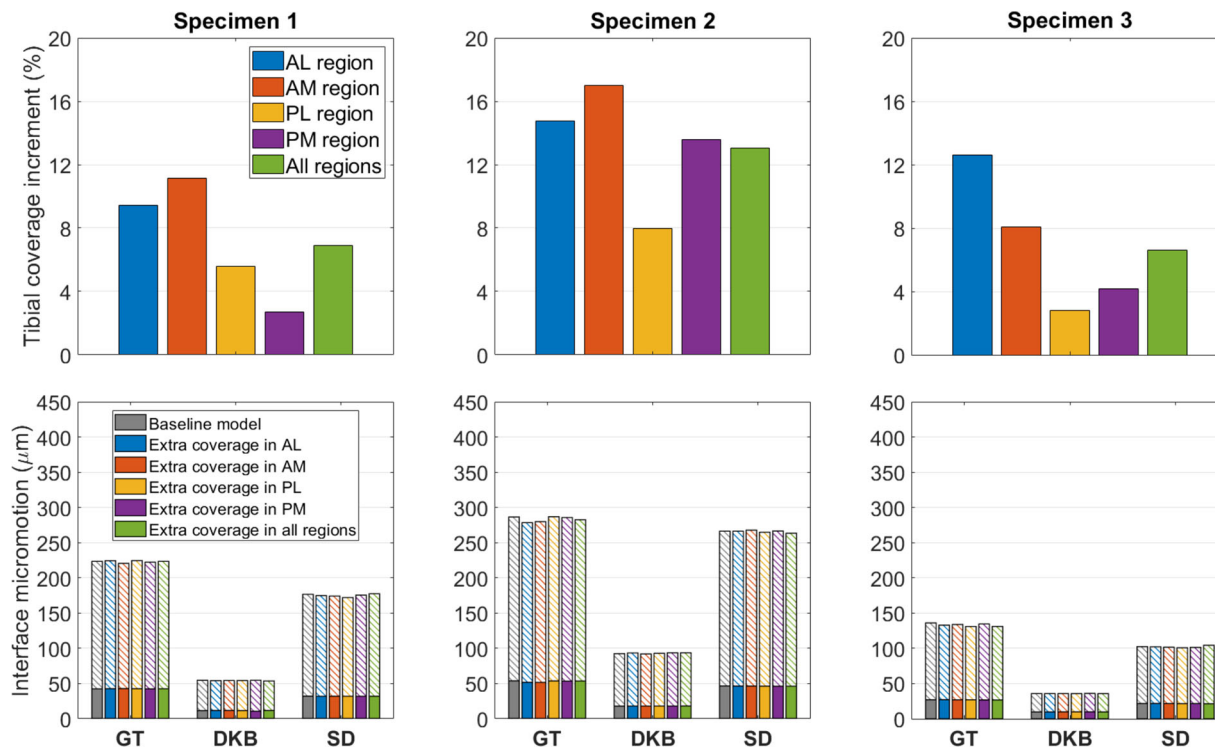


FIGURE 7 Tibial coverage increments in each region when using enlarged tray models (top). Comparisons of the interface micromotions between the baseline models and the models with extra tibial coverage (bottom). (AL, anterolateral; AM, anteromedial; PL, posterolateral; PM, posteromedial). The hatched bars represent the peak micromotions and the solid bars represent the average micromotions. [Color figure can be viewed at wileyonlinelibrary.com]

more sensitive to the factors studied than the shear micromotions (Figure 10).

4 | DISCUSSION

In this study, we investigated tray–bone interface micromotion during GT, DKB, and SD activities for three validated proximal tibial models. Specifically, we assessed the impact of seven common TKA factors on the interface micromotions. In all cases, the maximum micromotion always occurred at the anterior tray–bone contact interface, and no more than 50 μm micromotions were observed in the posterior regions except when a posterior resection error was created.

The tray–bone alignment had a significant impact on micromotions. We found that for the variability included, implanting the tray anteriorly, superiorly, or reducing the tibial varus alignment reduced the micromotion for all three specimens. Among these, the decrease in micromotion caused by the superior implantation was due to the increased tibial elastic modulus at the contact surface. When the change in surface modulus was small, the corresponding change in micromotion was also minimal (Figure 6—Specimen 2). The decrease in micromotion caused by anterior implantation was a result of the tray–bone contact locations also moving anteriorly, which centralized the load transfer with respect to the tibial shaft, reducing tibial bending and thereby reducing lifting of the tray at the anterior

aspect. The increase in micromotion caused by tibial varus alignment was due to the changes in medial-lateral load distributions. More varus alignments shifted the resultant contact force medially to the joint (Figure 3), increased the moment arm to the location of peak micromotion and resulted in more tray tilting at the anterolateral aspect. These findings were in line with previous studies.^{18,30} However, a previous study¹⁸ reported 79% increase in peak micromotion during the GT activity due to a 2° varus alignment, whereas the increment was approximately 13% with a similar perturbation in this study. The difference was thought to be because this study considered deformable polyethylene, and femoral-insert and insert-tray contact locations off the midline of the tray. The impact of tibiofemoral AP translation on the micromotion (which was found to be very sensitive) was reflected in our results. Finally, we found the micromotion was not sensitive to perturbation of the alignments along the other DoFs (ML, FE, and IE).

Similar to posterior positioning of the tray, posterior load transfer as a result of 100 N increases in posterior loading led to significant increases in micromotion. Again, this is the result of greater posterior offset of the load which maximizes the flexion-extension moment and anterior tray micromotion. Similarly, the micromotion was significantly increased during the DKB activity due to the considerable posterior offset of the load. Changes in micromotion were much smaller during GT and SD activities as the contact locations were minimally shifted in the AP direction (Figure 9C). The interaction here with articular design is important to note in that a geometry that

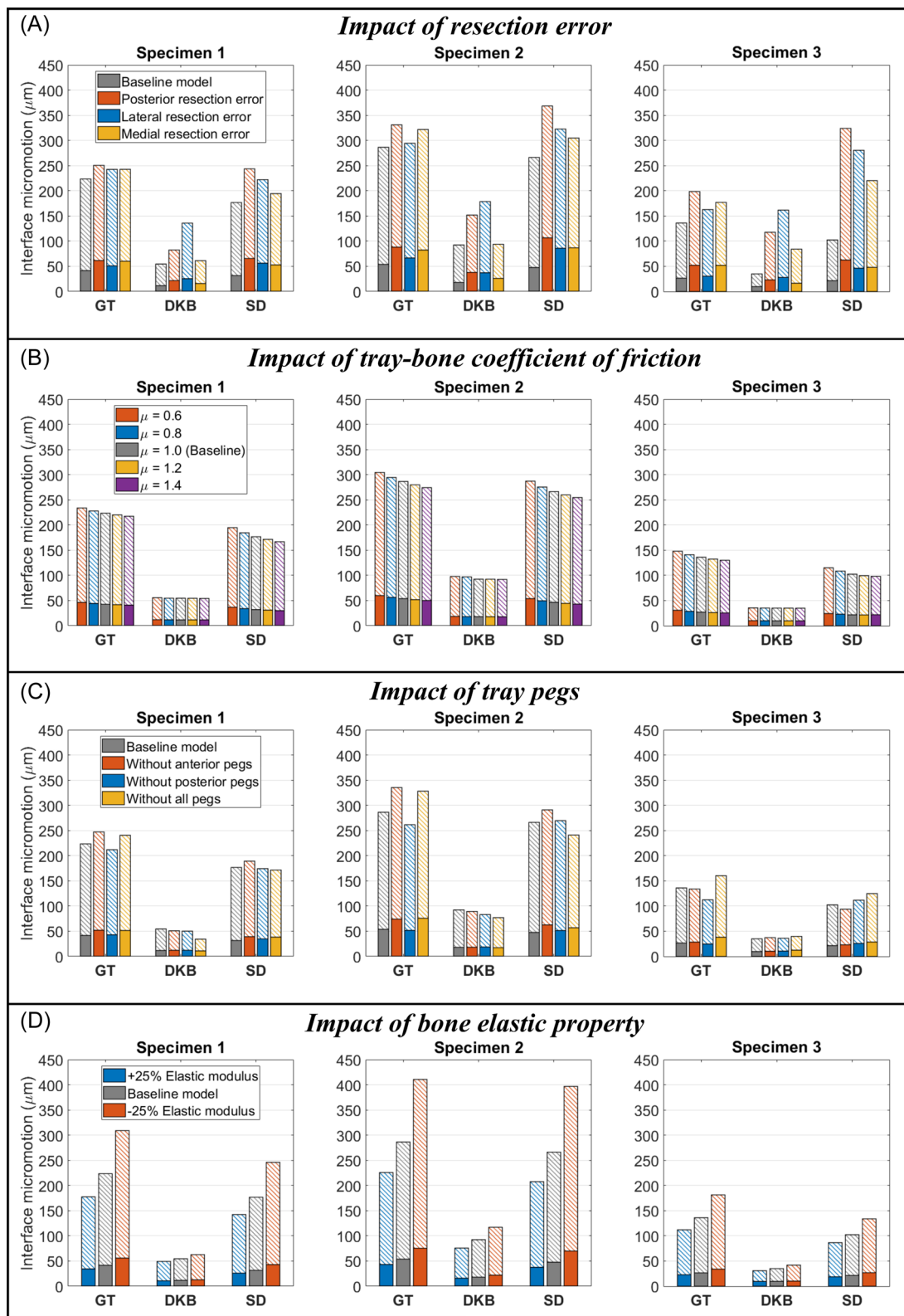


FIGURE 8 Impact of angular resection error (A), tray-bone coefficient of friction (B), tray pegs (C), and bone elastic property (D) on the interface micromotions. The hatched bars represent the peak micromotions and the solid bars represent the average micromotions. [Color figure can be viewed at wileyonlinelibrary.com]

TABLE 1 Ratio of the tray–bone cementless contact regions experiencing micromotion less than 50 µm to total bone–porous contact area

	Baseline model (%)	Model with angular resection errors (%)		
		Medial	Lateral	Posterior
Specimen 1				
Gait	74.1	53.3	64.6	53.0
Deep knee bending	99.9	99.7	83.3	91.4
Stair descent	80.2	54.6	60.0	49.0
Specimen 2				
Gait	70.3	49.1	56.5	41.6
Deep knee bending	93.9	85.4	71.9	69.7
Stair descent	75.0	47.5	52.3	38.9
Specimen 3				
Gait	84.6	56.0	80.9	58.3
Deep knee bending	100.0	97.5	80.4	85.6
Stair descent	90.7	65.4	67.6	53.9

Note: The minimal ratios were highlighted in bold.

constrains the load transfer more centrally will minimize the anterior micromotion.

This is in line with a previous study which denied the hypothesis that a relatively unconstrained articular geometry would result in less migration of the tibial component,³⁶ as peak micromotion appears primarily influenced by AP contact position and the resulting increase in moment about the anterior aspects of the tray.

Several studies have proposed that maximizing the tibial coverage should theoretically improve fixation performance due to the more uniform force distributions.^{19–21} However, we found that the extra coverage above a “best-fit” symmetric tray had a minimal impact on the micromotion. An average of 8.9% extra coverage only resulted in a 1.3% change in the micromotion. In addition, as it is impossible to obtain greater tibial coverage by optimizing the tray–bone alignment than using the virtual implant (which covered all the tibial resection surface) created in this study, the impact of maximizing the tibial coverage on the micromotion would be even smaller in clinical practice. In fact, choosing a larger tray to maximize coverage, but also simultaneously moving (as typical) contact locations posteriorly may even be counterproductive (in terms of reducing micromotion), as the influence of the posterior load transfer would increase micromotion. However, it should be noted that choosing a larger tray may influence cementless fixation in other aspects such as load transfer and bone strains. This evaluation also suggests that design efforts with respect to micromotion need not focus on maximizing coverage via tray asymmetry. Finally, note that this study did not focus on determining a minimum appropriate coverage, which should be further explored.

The uneven resection surface caused by angular cutting error during the tibial preparation had a moderate influence on the peak micromotion, as the peak micromotions at the anterior aspect did not increase greatly, indicating that the cone provides significant support compared with the tray surface. However, introducing large unsupported regions (Figure 4—resection error), led to a significant reduction in the ideal area for bone ingrowth (<50 µm) as expected.⁶ It should be noted that although the micromotions at those unsupported regions were mostly subsidence micromotions that resulted in gap-closing at the frame having the peak micromotions, the gap still recovered during each cycle with around 100 µm micromotion. Clearly, minimizing angular resection error at the posterior aspect is important as this pattern resulted in a minimal ideal area for bone ingrowth.

It should be noted that the implant used in this study was a rotating-platform design. The impact of tray pegs investigated here is not directly comparable to a typical fixed-bearing implant. We found that the anterior tray pegs inhibited micromotion, likely as the peak micromotions always occurred at the anterior aspect. However, overall, the pegs were responsible for only a small percentage of tray stability, as complete removal demonstrated an average increase of 13.3% of peak micromotion. The coefficient of friction also has only a small impact on the micromotion over a wide range studied, but clearly, intentional increase in friction will aid minimizing micromotion. Patient individual differences with respect to bone material properties had significant impact on the tray–bone interface micromotion. The differences in elastic modulus evaluated, up to 53% with the same bone volume fraction,²³ resulted in up to 74% differences in the micromotion.

This study has limitations to note. Only one implant design (rotating-platform and cruciate-retaining) was considered. The external boundary conditions and resulting sensitivities may be different for other implant designs. The impact of tray pegs investigated here is likely not reflective of the response for a fixed-bearing design. Future works could utilize the current computational framework to study other implant designs. This study evaluated the impact of the general variations in tibial material properties by perturbing the elastic modulus within the reported range. However, the impact of regional variations in material distributions and other patient factors (such as bone morphology) cannot be evaluated using only three subjects. We expect a follow-up study with a more comprehensive look at the regional variations of shape and elastic modulus.

In general, this study assessed the impact of seven common TKA factors on the tray–bone interface micromotion. Based on the results and discussion above, we ranked the impact of each factor on the peak micromotion from high to low in the following order: tibiofemoral posterior contact positioning, tray–bone alignment (AP and VV primarily), bone elastic properties, tibial angular resection error, the inclusion of tray pegs (anterior pegs having the greatest effect), tray–bone coefficient of friction, and tibial coverage. Among these, the impact of the tibial coverage was negligible. Tibial resection error was the most impactful to average micromotion as changes resulted in the highest average

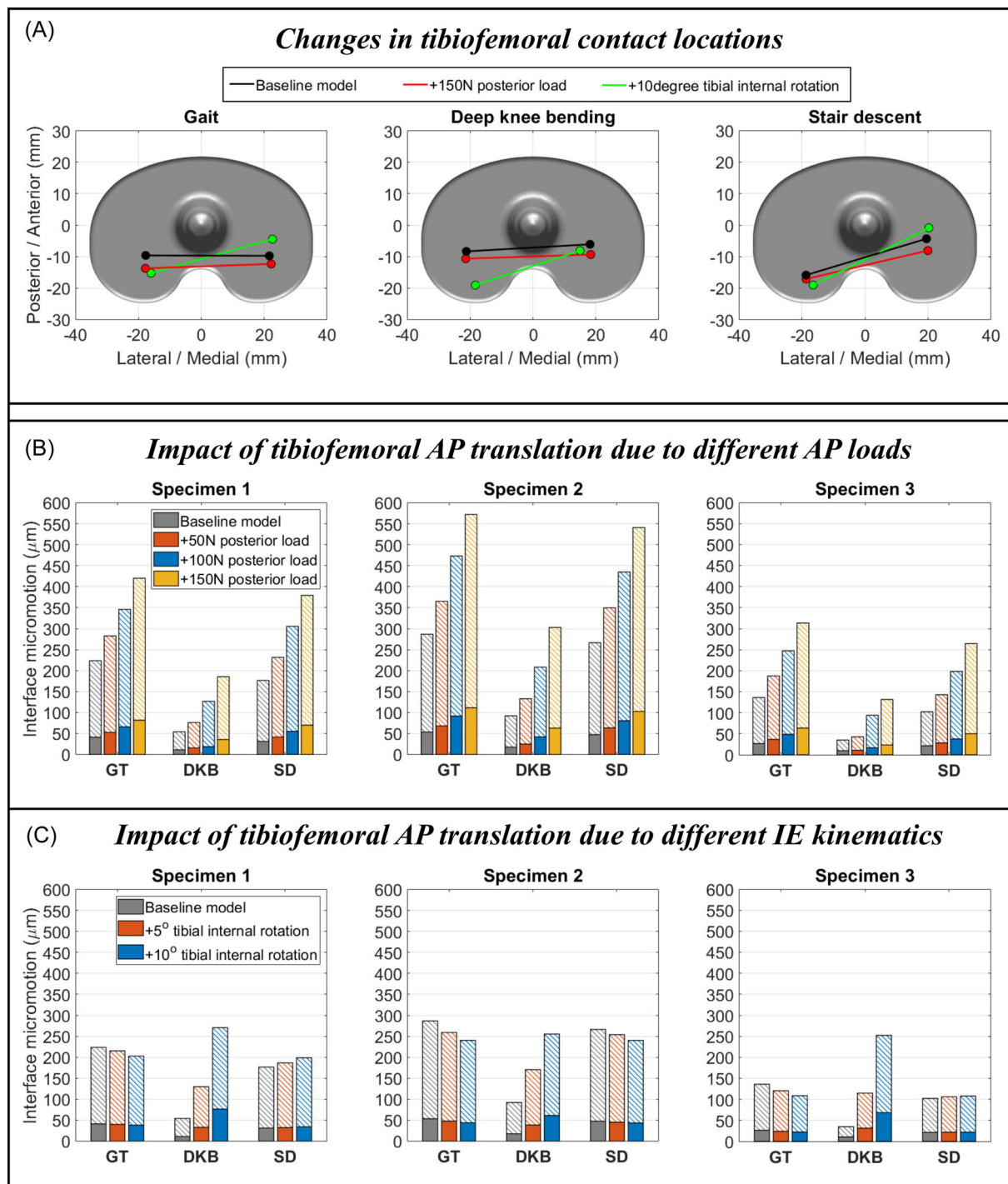


FIGURE 9 (A) Projection of the femoral-insert medial/lateral contact points (at the frame having peak micromotions) on the cementless tray for a left tibia specimen. (B) Comparison of the interface micromotions between the baseline models and the models with increased posterior loads. (C) Comparison of the interface micromotions between the baseline models and the models with increased tibial internal rotations. The hatched bars represent the peak micromotions and the solid bars represent the average micromotions. AP, anterior/posterior. [Color figure can be viewed at wileyonlinelibrary.com]

micromotion. The ranking is clearly dependent on the parameter settings evaluated for each factor. There are clear recommendations for minimizing micromotion from this assessment, including centralizing the load transfer where possible with tray positioning,

and less concern toward maximizing tibial coverage. However, as this is primarily a sensitivity screening study, critical parameters identified should be further explored to understand the potentially complex relationship with resulting micromotion. The study also

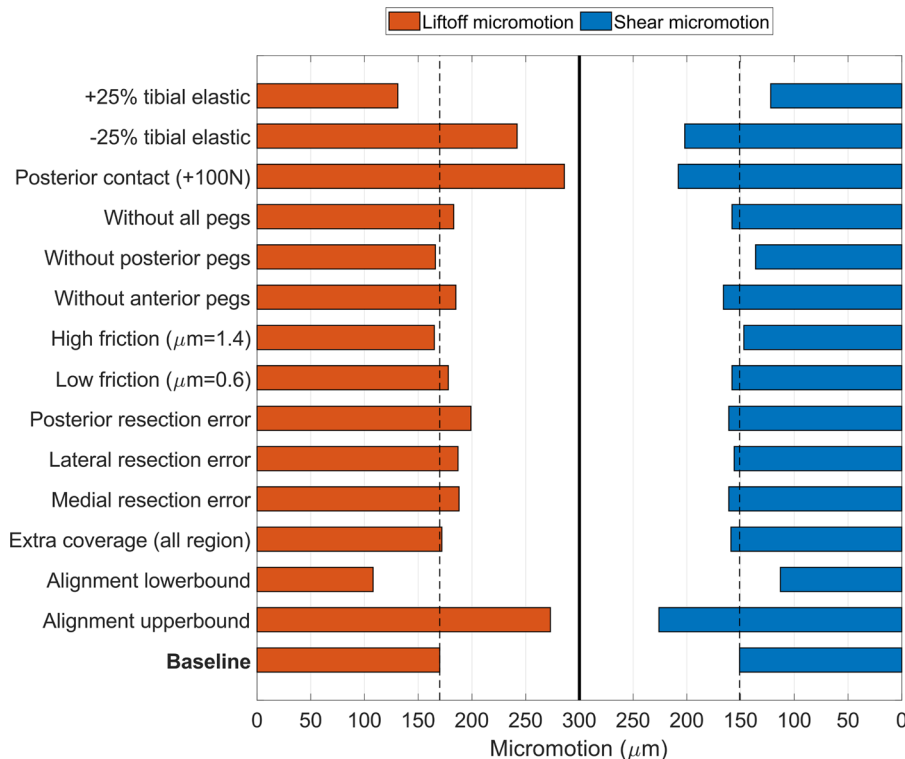


FIGURE 10 The normal and shear components of the total micromotion presented. (This reference plot is from the first specimen during gait activity.) [Color figure can be viewed at wileyonlinelibrary.com]

highlights the importance of articular design in that greater stability that centralizes the contact point will minimize micromotion.

AUTHOR CONTRIBUTIONS

Substantial contributions to research design, or the acquisition, analysis, or interpretation of data; drafting the paper or revising it critically; approval of the submitted and final versions: Yang. Substantial contributions to research design, or the acquisition, analysis or interpretation of data; approval of the submitted and final versions: Bayoglu. Substantial contributions to research design, or the acquisition, analysis or interpretation of data; approval of the submitted and final versions: Clary. Substantial contributions to research design, or the acquisition, analysis or interpretation of data; drafting the paper or revising it critically; approval of the submitted and final versions: Rullkoetter. All authors have read and approved the final submitted manuscript.

ACKNOWLEDGMENTS

This study was funded by DePuy Synthes Products, LLC.

CONFLICTS OF INTEREST

Authors (Paul J. Rullkoetter and Chadd W. Clary) received research or institutional support as a principal investigator from DePuy Synthes Products, LLC.

ORCID

Riza Bayoglu  <http://orcid.org/0000-0002-5481-3133>
 Chadd W. Clary  <http://orcid.org/0000-0002-5850-7096>
 Paul J. Rullkoetter  <http://orcid.org/0000-0003-3831-8623>

REFERENCES

- Aggarwal VK, Goyal N, Deirmengian G, et al. Revision total Knee arthroplasty in the young patient: is there trouble on the horizon? *J Bone Joint Surg.* 2014;96:536-542. doi:[10.2106/jbjs.m.00131](https://doi.org/10.2106/jbjs.m.00131)
- Aujla RS, Esler CN. Total knee arthroplasty for osteoarthritis in patients less than fifty-five years of age: a systematic review. *J Arthroplasty.* 2017;32:2598-2603. doi:[10.1016/j.arth.2017.02.069](https://doi.org/10.1016/j.arth.2017.02.069)
- Kim Y-H, Park J-W, Kim J-S. A comparison of 5 models of total knee arthroplasty in young patients. *J Arthroplasty.* 2016;31:994-999. doi:[10.1016/j.arth.2015.11.015](https://doi.org/10.1016/j.arth.2015.11.015)
- Dalury DF. Cementless total knee arthroplasty. *Bone Joint J.* 2016; 98-B:867-873. doi:[10.1302/0301-620x.98b7.37367](https://doi.org/10.1302/0301-620x.98b7.37367)
- Bragdon CR, Burke D, Lowenstein JD, et al. Differences in stiffness of the interface between a cementless porous implant and cancellous bone in vivo in dogs due to varying amounts of implant motion. *J Arthroplasty.* 1996;11:945-951. doi:[10.1016/s0883-5403\(96\)80136-7](https://doi.org/10.1016/s0883-5403(96)80136-7)
- Pilliar RM, Lee JM, Maniatopoulos C. Observations on the effect of movement on bone ingrowth into porous-surfaced implants. *Clin Orthop Relat Res.* 1986;11:11-11. doi:[10.1097/00003086-198607000-00023](https://doi.org/10.1097/00003086-198607000-00023)
- Engh CA, O'Connor D, Jasty M, McGovern TF, Bobyn JD, Harris WH. Quantification of implant micromotion, strain shielding, and bone resorption with porous-coated anatomic medullary locking femoral prostheses. *Clin Orthop Relat Res.* 1992;285:13-29. doi:[10.1097/00003086-199212000-00005](https://doi.org/10.1097/00003086-199212000-00005)
- Bhimji S, Meneghini RM. Micromotion of cementless tibial baseplates: keels with adjuvant pegs offer more stability than pegs alone. *J Arthroplasty.* 2014;29:1503-1506. doi:[10.1016/j.arth.2014.02.016](https://doi.org/10.1016/j.arth.2014.02.016)
- Small SR, Rogge RD, Malinzak RA, et al. Micromotion at the tibial plateau in primary and revision total knee arthroplasty: fixed versus rotating platform designs. *Bone Joint Res.* 2016;5:122-129. doi:[10.1302/2046-3758.54.2000481](https://doi.org/10.1302/2046-3758.54.2000481)
- Sukjamsri C, Gerald DM, Gregory T, et al. Digital volume correlation and micro-CT: an in-vitro technique for measuring full-field interface

- micromotion around polyethylene implants. *J Biomech.* 2015;48: 3447-3454. doi:[10.1016/j.jbiomech.2015.05.024](https://doi.org/10.1016/j.jbiomech.2015.05.024)
11. Camine VM, Rüdiger HA, Pioletti DP, Terrier A. Full-field measurement of micromotion around a cementless femoral stem using micro-CT imaging and radiopaque markers. *J Biomech.* 2016;49: 4002-4008. doi:[10.1016/j.jbiomech.2016.10.029](https://doi.org/10.1016/j.jbiomech.2016.10.029)
 12. Yang H, Bayoglu R, Renani MS, et al. Validation and sensitivity of model-predicted proximal tibial displacement and tray micromotion in cementless total knee arthroplasty under physiological loading conditions. *J Mech Behav Biomed Mater.* 2020;109:103793. doi:[10.1016/j.jmbbm.2020.103793](https://doi.org/10.1016/j.jmbbm.2020.103793)
 13. Chong DYC, Hansen UN, Amis AA. Analysis of bone-prosthesis interface micromotion for cementless tibial prosthesis fixation and the influence of loading conditions. *J Biomech.* 2010;43:1074-1080. doi:[10.1016/j.jbiomech.2009.12.006](https://doi.org/10.1016/j.jbiomech.2009.12.006)
 14. Taylor M, Barrett DS, Deffenbaugh D. Influence of loading and activity on the primary stability of cementless tibial trays. *J Orthop Res.* 2012;30:1362-1368. doi:[10.1002/jor.22056](https://doi.org/10.1002/jor.22056)
 15. Sopher RS, Amis AA, Calder JD, Jeffers JRT. Total ankle replacement design and positioning affect implant-bone micromotion and bone strains. *Med Eng Phys.* 2017;42:80-90. doi:[10.1016/j.medengphy.2017.01.022](https://doi.org/10.1016/j.medengphy.2017.01.022)
 16. Barker DS, Tanner KE, Ryd L. A circumferentially flanged tibial tray minimizes bone-tray shear micromotion. *Proc Inst Mech Eng.* 2005; 219:449-456. doi:[10.1243/095441105x34464](https://doi.org/10.1243/095441105x34464)
 17. Hashemi A, Shirazi-Adl A. 2000. Finite element analysis of tibial implants –effect of fixation design and friction model, computer methods in biomechanics and biomedical engineering. *Comput Methods Biomed Eng.* 3:183-201. doi:[10.1080/10255840008915264](https://doi.org/10.1080/10255840008915264)
 18. Glenday JD, Wright TM, Lipman JD, et al. Effect of varus alignment on the bone-implant interaction of a cementless tibial baseplate during gait. *J Orthop Res.* 2021;2021:1-10. doi:[10.1002/jor.25129](https://doi.org/10.1002/jor.25129)
 19. Bertin KC. Tibial component fixation in total knee arthroplasty. *J Arthroplasty.* 2007;22:670-678. doi:[10.1016/j.arth.2006.07.004](https://doi.org/10.1016/j.arth.2006.07.004)
 20. Wernecke GC, Harris IA, Houang MT, Seeto BG, Chen DB, MacDessi SJ. Comparison of tibial bone coverage of 6 knee prostheses: a magnetic resonance imaging study with controlled rotation. *J Orthop Surg.* 2012; 20:143-147. doi:[10.1177/230949901202000201](https://doi.org/10.1177/230949901202000201)
 21. Martin S, Saurez A, Ismaily S, Ashfaq K, Noble P, Incavo SJ. Maximizing tibial coverage is detrimental to proper rotational alignment. *Clin Orthop Relat Res.* 2014;472:121-125. doi:[10.1007/s11999-013-3047-y](https://doi.org/10.1007/s11999-013-3047-y)
 22. Plaskos C, Hodgson AJ, Inkpen K, McGraw RW. Bone cutting errors in total knee arthroplasty. *J Arthroplasty.* 2002;17:698-705. doi:[10.1054/arth.2002.33564](https://doi.org/10.1054/arth.2002.33564)
 23. Ulrich D, Hildebrand T, Van Rietbergen B, et al. The quality of trabecular bone evaluated with micro-computed tomography, FEA and mechanical testing. *Stud Health Technol Inform.* 1997;40:97-112. doi:[10.3233/978-1-60750-884-7-97](https://doi.org/10.3233/978-1-60750-884-7-97)
 24. Matsuda Y, Ishii Y. In vivo laxity of low contact stress mobile-bearing prostheses. *Clin Orthop Relat Res.* 2004;419:138-143. doi:[10.1097/00003086-200402000-00022](https://doi.org/10.1097/00003086-200402000-00022)
 25. Delport HP, Banks SA, De Schepper J, Bellemans J. A kinematic comparison of fixed- and mobile-bearing knee replacements. *J Bone Joint Surg.* 2006;88(8):1016-1021. doi:[10.1302/0301-620x.88b8.17529](https://doi.org/10.1302/0301-620x.88b8.17529)
 26. Navacchia A, Clary CW, Wilson HL, Behnam YA, Rullkoetter PJ. Validation of model-predicted tibial tray-synthetic bone relative motion in cementless total knee replacement during activities of daily living. *J Biomech.* 2018;77:115-123. doi:[10.1016/j.jbiomech.2018.06.024](https://doi.org/10.1016/j.jbiomech.2018.06.024)
 27. Anderson MJ, Keyak JH, Skinner HB. Compressive mechanical properties of human cancellous bone after gamma irradiation. *J Bone Joint Surg.* 1992;74(5):747-752. doi:[10.2106/00004623-199274050-00014](https://doi.org/10.2106/00004623-199274050-00014)
 28. Linde F, Hvid I, Madsen F. The effect of specimen size and geometry on the mechanical behavior of trabecular bone specimens. *J Biomech.* 1992;24(6):454. doi:[10.1016/0021-9290\(91\)90046-p](https://doi.org/10.1016/0021-9290(91)90046-p)
 29. Fitzpatrick CK, Maag C, Clary CW, Metcalfe A, Langhorn J, Rullkoetter PJ. Validation of a new computational 6-DOF knee simulator during dynamic activities. *J Biomech.* 2016;49:3177-3184. doi:[10.1016/j.jbiomech.2016.07.040](https://doi.org/10.1016/j.jbiomech.2016.07.040)
 30. Smith CR, Vignos MF, Lenhart RL, et al. The influence of component alignment and ligament properties on tibiofemoral contact forces in total knee replacement. *J Biomech Eng.* 2016;138(2). doi:[10.1115/1.4032464](https://doi.org/10.1115/1.4032464)
 31. Fitzpatrick CK, Baldwin MA, Clary CW, Maletsky LP, Rullkoetter PJ. Evaluating knee replacement mechanics during ADL with PID-controlled dynamic finite element analysis. *Comput Methods Biomed Eng.* 2012;17:360-369. doi:[10.1080/10255842.2012.684242](https://doi.org/10.1080/10255842.2012.684242)
 32. Snyder SM, Schneider E. Estimation of mechanical properties of cortical bone by computed tomography. *J Orthop Res.* 1991;9: 422-431. doi:[10.1002/jor.1100090315](https://doi.org/10.1002/jor.1100090315)
 33. Keyak JH, Lee IY, Skinner HB. Correlations between orthogonal mechanical properties and density of trabecular bone: Use of different densitometric measures. *J Biomed Mater Res.* 1994;28: 1329-1336. doi:[10.1002/jbm.820281111](https://doi.org/10.1002/jbm.820281111)
 34. Rho JY, Hobatho MC, Ashman RB. Relations of mechanical properties to density and CT numbers in human bone. *Med Eng Phys.* 1995;17:347-355. doi:[10.1016/1350-4533\(95\)97314-f](https://doi.org/10.1016/1350-4533(95)97314-f)
 35. Morgan EF, Bayraktar HH, Keaveny TM. Trabecular bone modulus-density relationships depend on anatomic site. *J Biomech.* 2003;36:897-904. doi:[10.1016/s0021-9290\(03\)00071-x](https://doi.org/10.1016/s0021-9290(03)00071-x)
 36. Uvehammer J. Knee joint kinematics, fixation and function related to joint area design in total knee arthroplasty. *Acta Orthop Scandinavica.* 2001;72:1-52. doi:[10.1080/000164701753759555](https://doi.org/10.1080/000164701753759555)

How to cite this article: Yang H, Bayoglu R, Clary CW, Rullkoetter PJ. Impact of patient, surgical, and implant design factors on predicted tray-bone interface micromotions in cementless total knee arthroplasty. *J Orthop Res.* 2022;1-15. doi:[10.1002/jor.25344](https://doi.org/10.1002/jor.25344)